Neuron, Volume *76*

Supplemental Information

Hilar Mossy Cell Degeneration Causes Transient

Dentate Granule Cell Hyperexcitability and

Impaired Pattern Separation

Seiichiro Jinde, Veronika Zsiros, Zhihong Jiang, Kazuhito Nakao, James Pickel, Kenji Kohno, Juan E. Belforte, and Kazu Nakazawa

Inventory of Supplemental Information

Supplementary Figures S1-S5

Supplemental Experimental Procedures

Supplemental References

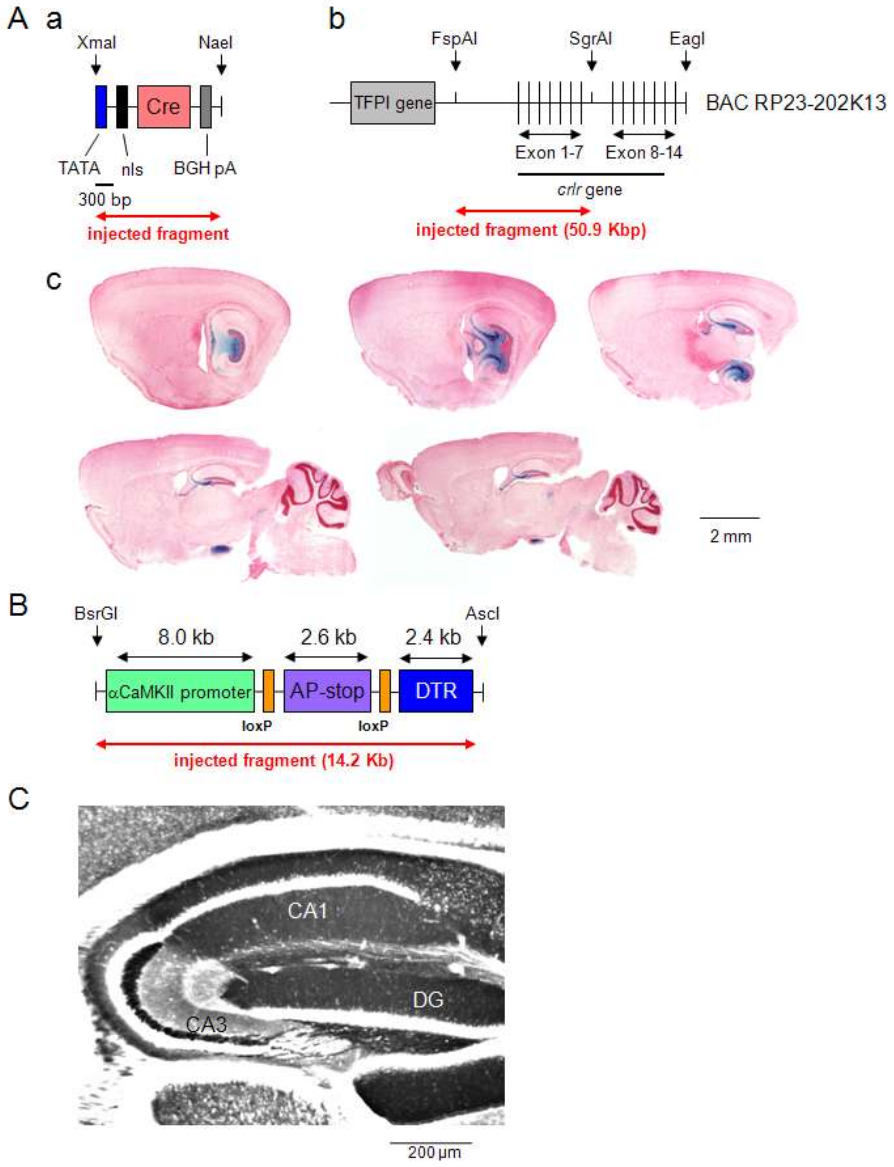

Figure S1. Generation of mossy cell/CA3-Cre line and CaMKIIα-floxed DTR line-B, related to Figure 1.

(**A**) Schematic of DNA constructs used for generation of Cre-transgenic line #4688 (a, b). Nls (nuclear localization signal)-Cre cDNA carrying HSP70 minimal promoter (a) and 50.9 kb DNA fragment separated from BAC clone RP23-202K13, which contains 5' transcriptional regulatory region of mouse calcitonin receptor-like receptor (crlr) as red underlined in (b), were co-injected into pronuclei of C57BL/6 mouse eggs. (c) X-gal staining in the brain of Cre line #4688 crossed to a *loxP*-flanked Rosa26*LacZ* reporter line. (**B**) (a) Schematic of DNA constructs (14.2 kb) injected for generation of *loxP*-flanked CaMKIIα-DTR transgenic mouse line-B. (b) Alkaline phosphatase staining using NBT/BCIP in the brain of *loxP*-flanked CaMKIIα-DTR line-B. AP, alkaline phosphatase; BGH-pA, the bovine growth hormone polyadenylation; nls, nuclear localization signal; TFPI, tissue factor pathway inhibitor. (**C**) An alkaline phosphatase-stained parasagittal section from the brain of floxed-diphtheria toxin receptor (fDTR) line-B (20-week-old). Note that the staining pattern in the CA3/hilar region is essentially the same as 8-week-old section (Figure 1D).

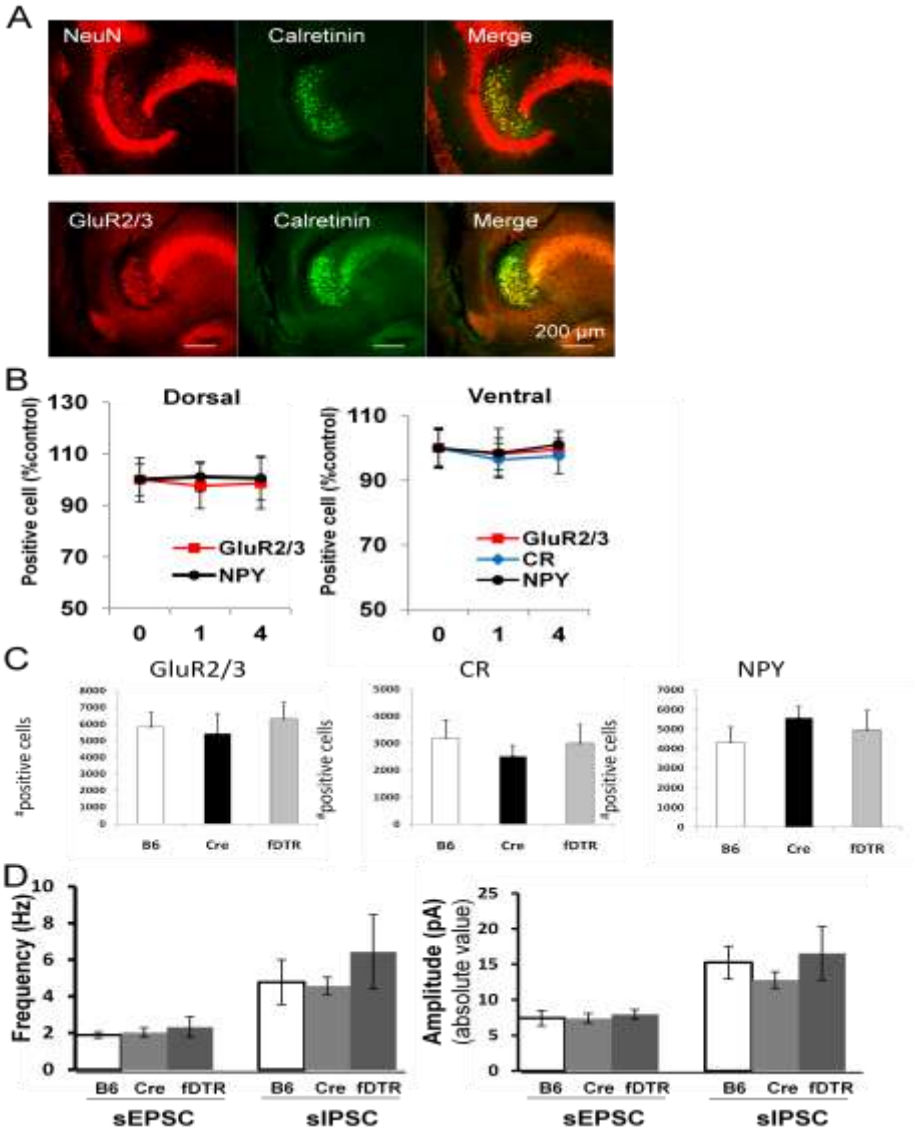

Figure S2. Immunocytochemical and physiological analyses (A, related to Figure 3B) Immunoreactivity against mouse ventral mossy cell marker, calretinin (CR), was fully overlapped with the labeling by anti-NeuN, or anti-GluR2/3(GluA2/3) on the fDTR control sections, suggesting that CR-positive cells and GluR2/3-positive cells originate from the same mossy cell population. (**B, related to Figure 3D**) DT treatment did not affect the number of hilar mossy cells or hilar interneurons in control mice. GluR2/3-, CR- and NPY-IRs were not significantly altered in the dorsal (left) and ventral hilus (right) of control mice after DT treatment. n=5 each for untreated, 1 week, and 4 week. (**C, related to Figure 3D**) DT treatment did not affect the number of hilar mossy cells or hilar interneurons among three control genotypes (n=4 each); C57BL/6 wild-type (B6), Cre-alone (Cre) and floxed-diphtheria toxin receptor alone (fDTR). The cell numbers positive for GluR2/3-, CR- and NPY-IRs in the hilar region of one hemisphere were not significantly altered 4 weeks after DT treatment. One-way ANOVA; CR ($F(2,12)=0.903$, $p=0.436$), GluR2/3 ($F(2,10)=0.304$, $p=0.744$), and NPY ($F(2,10)=1.759$, $p=0.222$). **(D. related to Figures 4A and 4B)** DT treatment did not affect the properties of sEPSCs and sIPSCs among three control genotypes during acute phase (animal number n=5 for B6, n=4 for Cre, n=4 for fDTR). One-way ANOVA, $p=0.72$ for sEPSC frequency, $p=0.72$ for sIPSC frequency, $p=0.87$ for sEPSC amplitude, $p=0.50$ for sIPSC amplitude.

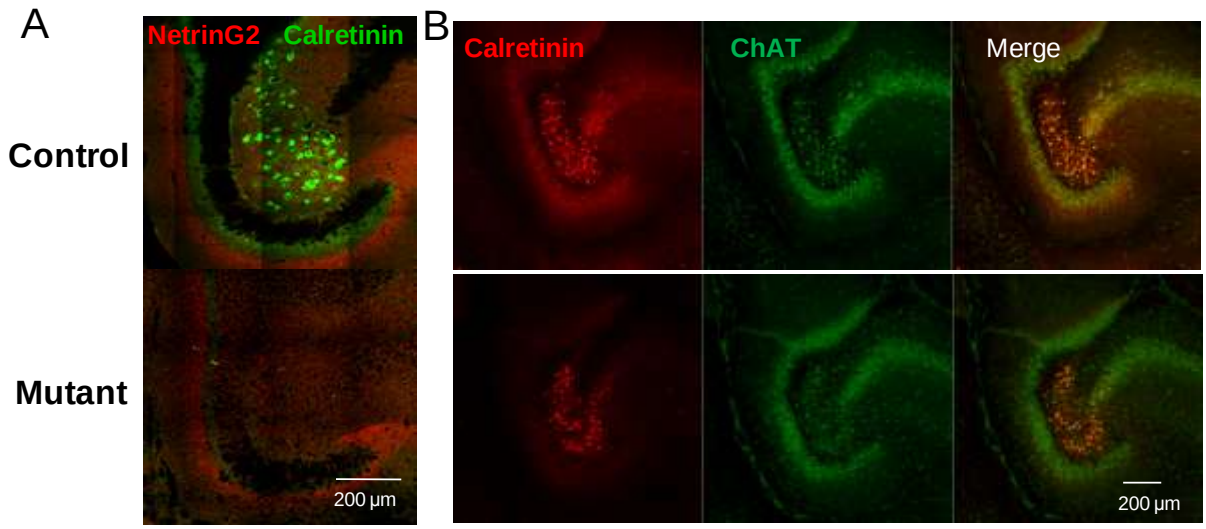

Figure S3. Perforant path projection and cholinergic innervation, related to Figure 6.
(A). Double immunostaining of Netrin G2 (red, marker for perforant path axons) and calretinin (green, marker for mouse mossy cell) in the ventral hippocampus of control (top) and mutant (bottom) mice, showing no change in perforant path projections after mossy cell degeneration. (**B).** Double immunostaining of choline acetyltransferase (ChAT, green) and calretinin (red) in the ventral hippocampus of control (top) and mutant (bottom) mice. Since ChAT-immunoreactive neurons are rare in the hippocampus (Frotscher et al., 1986), these ChAT staining largely represent a dense plexus of cholinergic fibers. Despite extensive mossy cell degeneration (over 70% mossy cell loss in the mutant), ChAT-positive plexuses (see 'green signals' in the merged image in the mutant hilar region) were visible in the hilar region and no robust change was observed between genotypes after DT treatment. We did not see any sign of retraction of cholinergic projection by the mossy cell loss.

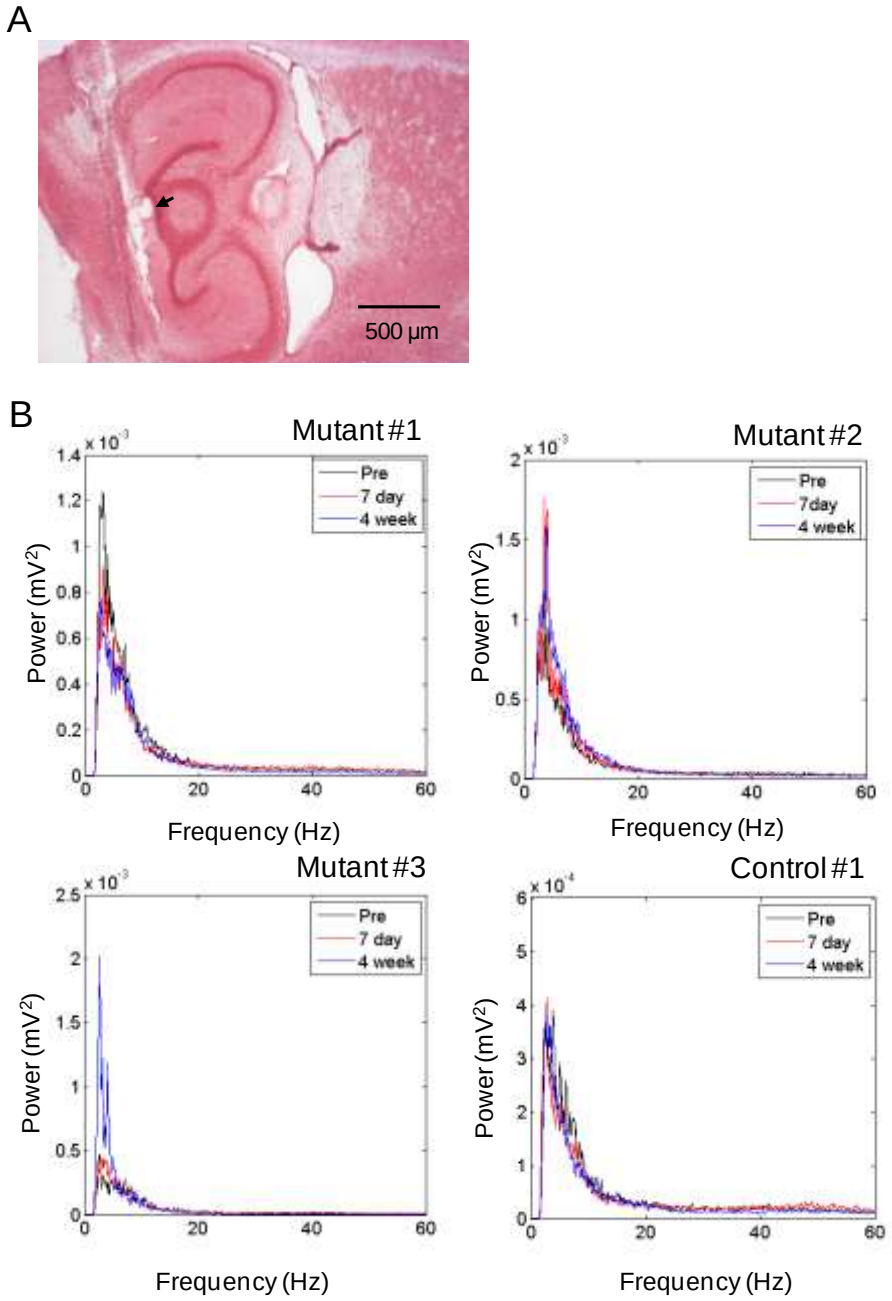

Figure S4. *In vivo* analysis of dentate LFP oscillatory activity, related to Figure 7.
(A), Representative Nissl-stained parasagittal section showing an example of the location (arrow) of the recording electrode implanted in the dentate granule cell layer for LFP analysis. After the recordings in the chronic phase were completed, the recording sites were microlesioned by current injection to verify the location of the multi-electrodes. Mice were then perfused with 4% paraformaldehyde for Nissl staining. (**B).** Averaged LFP power spectra of individual animals obtained from the same electrodes located in the dentate gyrus during immobility periods (5-min epochs x 2) of just before DT treatment (Pre), 7 days (7 Day) and 28 days (4 weeks) after DT treatment. There were no consistent changes in the LFP power spectra before and after DT treatment regardless of the genotypes. Only one animal data is shown for control genotype because no obvious changes were detected in other two control mice as well.

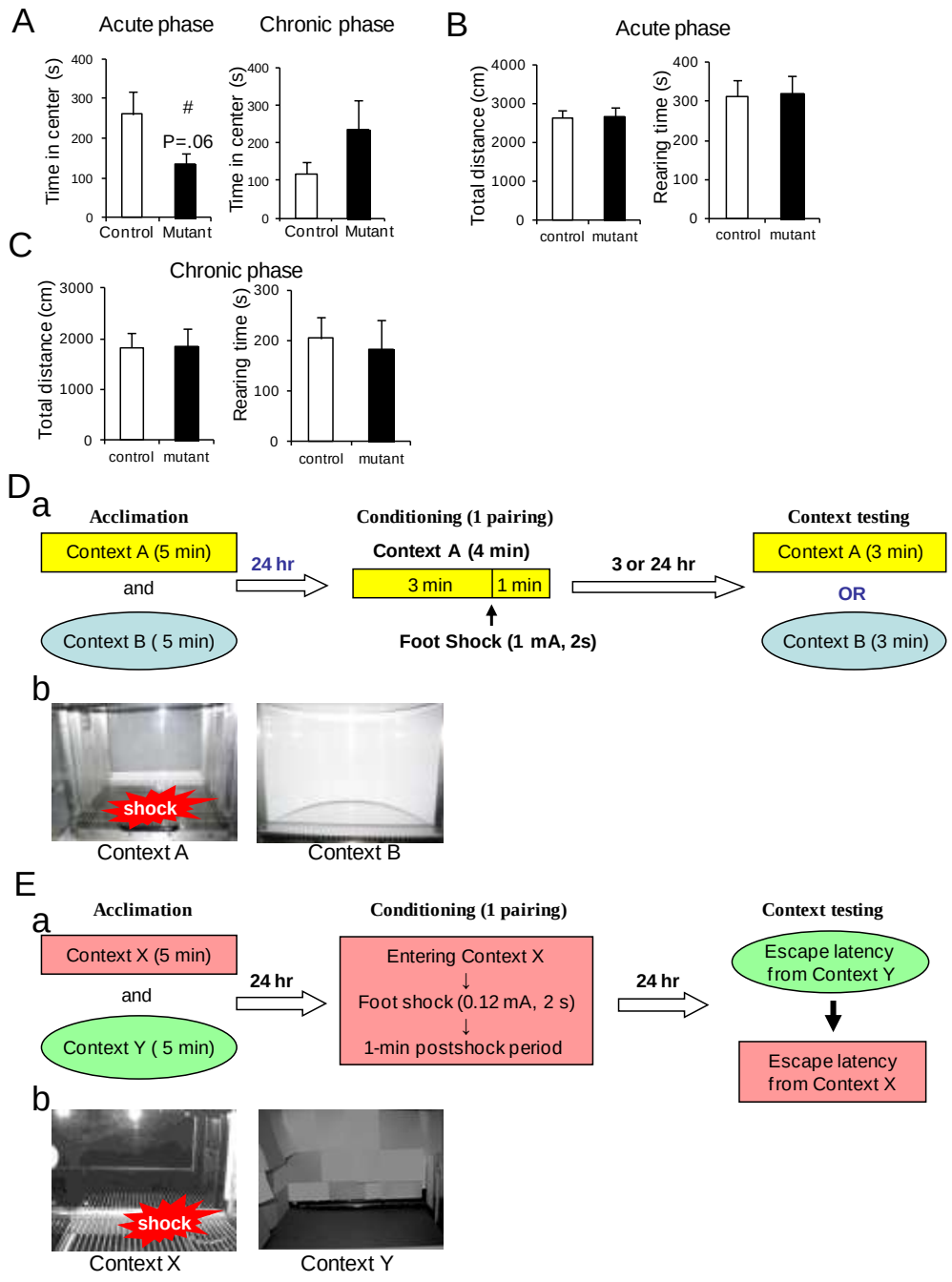

Figure S5. Behavioral characterization after mossy cell degeneration, related to Figure 8.
(**A-C**) Locomotor activity in an unfamiliar open field for 30 min in acute phase or in chronic phase following mossy cell degeneration. A tendency of mutant anxiety-like behavior was detected in acute phase (260.9 ± 57.7 s for control, 134.4 ± 28.8 s for mutant, Student's *t*-test, #*p*=0.06), but not in the chronic phase (A). No differences were observed in total distance and rearing time between genotypes in acute (B) or chronic phase (C). n=12 for each genotype. (**D**) Procedure of pattern separation task using one-trial contextual fear conditioning. (a) Schematic of one-trial contextual fear conditioning. (b) Photo of context A (left) and context B (right). (**E**) Procedure of pattern separation task using one-trial step-through active avoidance. (a) Schematic of one-trial step-through avoidance. (b) Photo of context X (left) and context Y (right).

Supplemental Experimental Procedures

All experimental procedures were carried out in accordance with the National Research Council's Guide for the Care and Use of Laboratory Animals, and were approved by the NIMH Animal Care and Use Committee. Data are presented as mean ± SEM. All of the experiments were conducted by operators who were blind to the mouse genotypes.

Generation of Double Transgenic Mice

To generate mossy cell-Cre lines, a 50.9 kb FspAI-SgrAI DNA fragment containing the 5'-transcriptional regulatory region of the mouse calcitonin receptor-like receptor (*Crlr*) was separated from the BAC clone, RP23-202K13 (BACPAC Resource Center, Children's Hospital Oakland Research Institute), and this fragment was co-injected with nuclear localization signal (nls)-Cre cDNA, carrying HSP70 minimal promoter into pronuclei of C57BL/6N mouse eggs (Figure S1A). Note that we obtained this Cre line serendipitously, perhaps due to the unspecified combination effect of putative enhancer/silencer in the fragment and the integration site into the genome. A co-injection strategy might also have also increased a possibility of obtaining Cre expression patterns independent of 5'-transcriptional regulatory elements of CRLC gene. We found this line out of 15 transgenic lines, and no other lines showed similar Cre expression patterns. The following PCR primer set, which produces a 375 bp band, was used to identify transgene-positive mice: 5'-AGAGGCGCTTCGTCTACGGAGCGACAATTC-3' (HSP promoter primer), and 5'-CTCATCACTCGTTGCATCGACCGGTAATGC -3' (Cre-27 antisense). Cre recombination pattern was characterized by crossing to *loxP*-flanked Rosa26*LacZ* reporter mice as previously described (Jiang et al., 2010). We also generated *loxP*-flanked diphtheria toxin receptor (fDTR) transgenic lines in which following Cre-mediated recombination, human heparin-binding epidermal growth factor–like growth factor (HB-EGF, I117V/L148V mutant), was expressed under the control of the murine CaMKIIα promoter (~8.0 kb). This mutant HB-EGB functions as a DTR with no epidermal growth factor-like activity (Furukawa et al., 2006). In addition, human alkaline phosphatase cDNA was transcribed before recombination, allowing the transgene expression pattern to be evaluated by alkaline phosphatase staining (Figure S1B). The following PCR primer set, which produces a 286 bp band for non-recombination allele and/or a 422 bp band for recombination allele, was used to identify transgene positive mice: 5'-ACTCCCAGGTCCAACTGCAG-3' (DTR primer A), 5'-TCAACTAGGATGATGCCCAG-3' (DTR primer B) and 5'-AATATACCCTGATTGCCTTG-3' (DTR primer C).

To generate mossy cell-DTR mutant mice, from the multiple Cre and fDTR lines created we intercrossed a Cre line (#4688) with a fDTR (line-B), thus generating mutant mice (Cre $^{+/-}$; fDTR $^{+/-}$) and three control littermates (hemizygous fDTR-line B, hemizygous Cre, and wild-type mice) on a C57BL/6NTac (B6) background. All of these groups were treated between the ages of 12 to 20 weeks with diphtheria toxin (DT, *i.p.* injection at 25μg/kg per day, Sigma #D0564) or saline for 2 consecutive days. Except for the histological characterization of Cre mice, the data from the three control genotypes were combined into a single control group because there were no significant differences found in the histological analyses, slice physiology, *in vivo* recording or behavioral experiments. To assess the impact of DT treatment on the DTR-positive cell viability, the mutants were further crossed with *loxP*-flanked Rosa26*LacZ* reporter mice. All the experiments were conducted by researchers who were blind to the genotypes of the mice used.

Histological Procedures

Immunohistochemistry

To characterize Cre-expression, 40 μm-thick brain sections of 8-12 weeks old Cre/*loxP*-flanked Rosa26*LacZ* double transgenic mice were stained with the following primary antibodies: mouse anti-β galactosidase (1:2000, Z3781, Promega) and rabbit anti-Cre (1:1000, 69050-3, Novagen). To evaluate the DT-induced histological change in mutant and control mice, their brains were fixed 4 to 7 days (acute

phase) or 4 to 6 weeks (chronic phase) following DT treatment (n=5 each). The brains of untreated mutant and control mice (n=6 each) were fixed immediately at day 0. Brain sections were subjected to immunostaining with the following primary antibodies: rabbit anti-calretinin (1:2000, AB5054, Chemicon, Temecula, CA), mouse anti-calretinin (1:200, Clone: Z11-E3, Invitrogen), mouse anti-GAD67 (1:5000, MAB5406, Chemicon), rabbit anti-GluR2/3(GluA2/3) (1:200, AB1506, Chemicon), mouse anti-NeuN (1:1000, clone A60, Millipore), rabbit anti-neuropeptide Y (1:1000, CURE/Digestive diseases research center UCLA, CA), goat anti-choline acetyltransferase (1:200, AB144P, Millipore), rabbit anti-netrin G2 (1:100, from S Itohara, Riken BSI, Japan). The number of immuno-positive cells were counted from four parasagittal sections per mouse, divided by the area of hilus, and averaged per mouse. The group averages for genotype/time point were normalized against the untreated animals to calculate the percent change relative to the control value. Nissl staining was conducted using Safranin-O.

For assessing the NeuN-positive cell number, three parasagittal sections showing ventral hippocampus (lateral 2.725 mm to 2.525 mm from bregma) were chosen. NeuN-positive cell number was then counted both in the CA3c pyramidal cells, which are flanked by the upper and lower dentate blades in the dentate hilus (Lorente de No, 1934) of ventral hippocampus. The data were averaged per mouse (n=4 for each genotype/treatment).

To evaluate dentate excitability 1 hr after KA injection (20 mg/kg *i.p.*) in acute (n=8 for each genotype) and chronic phase (n=6 for mutant, n=4 for control), rabbit anti-c-Fos (1:20,000, PC38, Calbiochem) and rabbit anti-zif268 (1:7500, sc-110, Santa Cruz Biotechnology) were used with a HRP-conjugated anti-rabbit secondary antibody. The number of DAB-positive cells was counted from three parasagittal sections per mouse, divided by the area of dentate granule cell layer, and then averaged per mouse. The group averages from genotype/time point were compared using the Student's *t*-test.

GAD67-IR in IML of the dentate gyrus after DT treatment was rated with a modified scale of Tauck and Nadler (1985) according to a 0–3, semiquantitative scale: 0, no or occasional inner molecular layer staining; 1, scattered staining above all parts of inner molecular layer; 2, continuous intermediate or patchy heavy staining; 3, continuous heavy staining.

Timm's Staining

Four to 6 weeks after DT treatment, mutant (n=6) and control (n=5) mice were perfused with 0.37% sulphide solution for 5 min followed by 4% paraformaldehyde for 5 min. Mounted sections were covered with a developer, which consists of 50% gum arabic solution, 2 M citrate solution, 5.67% hydroquinone solution and 17% $AgNO_3$ solution, for 1 hr in a dark room, and subsequently washed in tap water (Sloviter, 1982).

Kainic Acid-Induced Seizure and Behavioral Seizure Scoring

Mutants (n=8 for acute phase and n=7 for chronic phase) and controls (n=8 for acute phase and n=5 for chronic phase) received kainic acid (KA, Tocris, Ellisville, MO) with 20 mg/kg *i.p.* and seizure activity was behaviorally monitored for 1 hr and scored as described previously (Jinde et al., 2009).

Slice Physiology

Whole cell recording:

Horizontal slices containing the ventral hippocampus (350 μm thick) were cut from the mutant mouse line and their littermates (12-20 weeks old). Dentate granule cells were visualized with an upright microscope equipped with a 40x infrared immersion DIC objective coupled to a monochrome digital camera. Spontaneous events were collected from the granular cells using conventional whole cell recording techniques with a Multiclamp 700B amplifier connected to a 1322 A/D board and Clampex 10 program suite (Molecular Devices, Sunnyvale, CA). Access resistance was monitored by injecting 5 mV steps throughout the experiment. Intracellular solution contained (in mM):

125 Cesium-methane-sulfonate, 4 ATP-Mg_2, 4 NaCl, 0.3 GTP, 16 $KHCO_3$, 5 N-2(2,6-dimethylphenylcarbamoylmethyl)triethylammonium chloride (QX-314-Cl) and equilibrated with 95% O2 and 5% CO_2 to pH 7.3. The final osmolarity was 270-290 mOsm. The liquid junction potential was subtracted off-line and included in all the holding potential values throughout the paper. Spontaneous

excitatory postsynaptic events were collected in voltage clamp mode at a holding potential value of -67 mV and they occurred as inward events, while inhibitory postsynaptic events were collected at +3 mV as outward events in the same experiments at a temperature of 32-34 °C. Spontaneous events were first collected in 60-s long traces using the template-based analysis feature of Clampfit 10.0. Events with peak amplitude values at least of 2-fold the standard deviation were included in the sample population. At a holding potential of -67 mV only excitatory events were detected, because GABA reversal potential was measured to be -69.6 mV in the presence of 20μM 6-nitro-7-sulfamoylbenzo(f)quinoxaline-2,3-dione (NBQX), 50 μM D-AP5 and 1 μM CGP55845 (N=6 experiments). Similarly, at a holding potential of +3 mV no events were detected in the presence of 20 μM NBQX, 50 μM APV, 1 μM CGP55845 and 12.5 μM gabazine (SR-95531) (n=6 experiments). Genotype and time period after DT-treatment did not affect reversal potential values: -70.6 ± 1.05 mV, -69.6 ± 1.72 mV, -71.8 ± 0.93 mV, and -69.6 ± 1.00 mV [one week after DT treatment control (n=6) and mutant (n=5), 6 weeks after DT treatment control (n=6) and mutants (n=5), respectively]. Access resistance was monitored with 5 mV steps and data from experiments were excluded if the access resistance or the input resistance changed more than 20% during the experiment.

Field potential recording

To evaluate changes in the dentate gyrus excitability we collected fEPSP and population spike recordings in 400-μm horizontal slices of the hippocampus in current clamp mode. Patch pipettes were filled with oxygenated ACSF and placed at the border of granular cell layer and inner molecular layer. The field potentials were low-pass filtered at 10 kHz and sampled at 10 or 20 μs. A concentric bipolar electrode with a diameter of 200 μm (#CBBRC75, FHC instruments, Bowdoin, ME) was placed on the surface at the most temporal part of the dentate outer molecular layer to electrically stimulate perforant path. The stimulus, which has a width of 0.02 ms for fEPSP collection and 0.05 ms for the collection of population spikes, was delivered at a frequency of 0.1 Hz with the help of an Iso-flex stimulus isolation unit (A.M.P.I, Jerusalem, Israel) triggered from Clampex. Stimulus intensities were about 1, 2.5, 5, 7.5, and 10 V. Five to 15 traces were collected at every stimulus intensity level, and then averaged for evaluation. Only experiments that yielded monosynaptic fEPSP and visible fiber volley with at least 2 different stimulus intensities were included in the data set. To account for the variability of the number of fibers stimulated, we normalized fEPSPs with fiber volley values. Since higher stimulus intensities often generated population spikes (Toth et al., 1997), fEPSPs with visible population spikes were not used in the analysis. Fiber volleys and fEPSP amplitudes were measured as a maximum voltage difference from the baseline. At every stimulus intensity amplitudes were normalized to the fiber volley values in order to avoid a possible bias coming from stimulating a different amount of fibers from the different slices. To find the average fEPSP amplitude/fiber volley for every experiment, fEPSP amplitude was plotted as a function of the fiber volley and fitted with a straight line during the linear increase phase. We calculated the slope of this line from 1-4 slices from every animal. To ensure that we recorded fEPSPs, 20 μM NBQX and 50 μM D-AP5 was applied at the end of the experiments and completely blocked the fEPSP while the fiber volley stayed stable (n=5).

We also measured the stimulation threshold change for population spikes after mossy cell ablation as a marker of excitability increase. The perforant path stimuli, with a width of 0.05 ms at 0.1 Hz and an intensity of 1, 2.5, 5, 7.5, or 10 V, generated population spikes in 87% of all experiments. Notably, higher stimulus intensities sometimes produced a single small-amplitude discharge (but occasionally doublets or very rarely triplets) riding on the population spikes (field potentials). For example, when stimulated with an intensity of 5V, such ride-on discharges were detected in 33% (6/18) of the experiments one week after DT treatment in the mutants, whereas such discharges were detected only in 7%, 9%, and 6% of the experiments in chronic mutants, acute controls, and chronic controls, respectively. When stimulated with an intensity of 7.5 V, the ride-on discharges were detected in 39% (7/18) of the experiments one week after DT treatment in the mutants, whereas such discharges were detected only in 11%, 5%, and 17% of the experiments in chronic mutants, acute controls, and chronic controls, respectively. These results may also suggest a granule cell excitability increase in the mutants during the acute phase after DT treatment. However, over 60 % of the experiments in acute phase-mutants displayed

no such discharges, and in those that did these events were canceled out after these 5 to 15 traces were averaged. We have rarely observed high-frequency multiple population spikes in any conditions. As additional measure of excitability, we calculated population spike amplitudes at multiple stimulus strengths. We found that there was a significant difference in the population spike amplitudes at medium stimulus strength at 7.5 V. In this case, right after mossy cell degeneration we observed a 0.90±0.24 mV populations spike in the mutants, with compared to 0.28±0.075, 0.34±0.09, and 0.30±0.07 for acute control, and chronic controls and mutants, respectively, ANOVA, $F(3,80)=5.22$, $p<0.05$). However, there were no significant differences among genotypes/conditions at lower stimulus strength at 2.5 V and higher stimulus strength at 10 V related to saturation. Therefore, we simply measured a minimum stimulus intensity among 1, 2.5, 5, 7.5, or 10 V that was sufficient to generate at least one population spike and scored as population spike threshold. In those cases where no population spike was generated we arbitrarily given a threshold value of 12.5 V. We collected the data from 2-6 slices from each animal then created a population spike threshold value per animal.

***In Vivo* Local Field Potential Recording**

LFP recordings were taken just before and several time points after DT injection (n=8 for control, n=9 for mutant), as described previously (Jinde et al., 2009) with modifications. A microwire array consists of 7 Formvar-insulated nichrome wires (50 μm in diameter; #762000, AM system, Carlsborg, WA, USA), which were aligned in a single slanted row to vary the depth of recording, with an inter-electrode separation of 50-100 μm. Each microwire was connected with a silver paint to the pin of an 8-pin subminiature headpiece connector (Mill-Max Mfg. Corp., Oyster Bay, NY, USA) and securely covered by polyester shrink tubing. One pin was bent to attach an enamel-coated copper ground wire (255 μm in diameter) to the skull during the surgery. All the connection points were finally sealed and stabilized with a thin layer of dental acrylic. The impedance of each electrode wire tip was between 0.2 to 0.5 MΩ. The microwire array was surgically-implanted on the skull in the right hemisphere (Stereotaxic coordinates from bregma: 2.7 mm lateral; 3.0-3.8 mm posterior) with the electrode tips at a maximum depth of 3.7 mm below the cortical surface so as to be located from the corpus callosum to the ventral dentate gyrus. After 10 days of recovery, LFP recordings were taken a few hrs before DT injection as well as 1, 2, 3, 5, 7, 14, 28, and 35 days after the first DT injection as the mice navigated a circular open arena (45-cm diameter) for 2-3 hr. LFP signals were filtered (bandwidth from 0.1 to 475 Hz), digitized, and acquired at a sampling rate of 1.56 kHz per channel, using Cheetah-64 recording system (Neuralynx Inc.). Epileptic activity of these mice was also behaviorally observed for at least 4 hr before and 1-2 hr after LFP recording (total ~8 hr per day). The LFP signals were analyzed off-line with NeuroExplorer 4 software (Nex Technologies, Littleton, MA). An epileptic LFP activity was also obtained from the electrodes placed in CA1 pyramidal cell layer of B6 mice treated with KA (20 mg/kg, *i.p.*).

For the analysis of dentate LFP oscillations, we analyzed the LFPs recording from the electrodes located in the dentate granule cell layer or hilar region, which was estimated by the by the distance (> 100 μm) from the polarity reversal of the "dentate EEG spikes" during immobility (Bragin et al., 1995b; Buzsáki et al., 2003) and further verified by electrolesions. The immobility period was defined by the simultaneous tracking of the small infrared light-emitting diodes (LEDs) mounted on the animal headstage with no displacement of LED position more than 3 cm within a second. The putative REM stage periods, assessed by the large amplitudes of theta oscillations, were excluded from the analysis. The criterion for detecting dentate spikes was large-amplitude positive spikes (exceeding mean±2SDs from the amplitudes of the "background" LFPs during a 5-min immobility period at the end of each session) of 10-40 ms duration (Bragin et al., 1995b; Penttonen et al., 1997). Recordings from the granule cell layer or the hilus were also confirmed by the presence of large-amplitude theta oscillations during the exploration (Bragin et al., 1995a; Buzsáki et al., 2003) where the LED moved around continuously over 1 min. Notably, mossy cell degeneration did not affect animal locomotor activity (see Figure S5B-C). We only included animals (n=3 for mutants, n=3 for fDTR controls), in which voltage-versus-depth profiles of hippocampal field activity was consistent across the recording dates before and after DT injections and where the polarity reversal point of the dentate spikes was unambiguously identified. For theta frequency

oscillation (bandwidth; 7-12 Hz), 5-15 epochs of 1-min exploration were collected during exploration periods. These data were applied by 2-Hz high pass filter, analyzed with power spectrum density (1024 frequency values), and averaged per animal. For gamma frequency oscillations during exploration, the same data as in the theta frequency oscillation analysis were averaged at 30-100 Hz bandwidth. However, no significant changes were detected in the gamma oscillations across days (data now shown). LFP spectrogram was calculated off-line. Neuralynx LFP files were converted to Neuroexplore (Ver.4.109, Nex Technologies, Littleton, MA) and Matlab (Ver.7.12. MathWorks, Natick, MA) files.

Mouse Behavior

Behavioral Tests for Contextual Discrimination

Mice 5-7 days after DT treatment (in acute-phase: n=20 for control; n=22 for mutant) were subjected to one-trial contextual fear conditioning to assess pattern separation, as previously described (Cravens et al., 2006). In a separate cohort, mice 4-6 weeks after the treatment (chronic phase; n=16 for mutant and control, respectively) were also subjected to the same task. Briefly, 3 or 24 hr after receiving to a foot-shock (2 s, 1.0 mA) in Context A, mice were divided into two groups and freezing behavior (quantified by FreezeView (Actimetrics Software, Evanston, IL, USA) was measured in either the same context (Context A) or in a different context (Context B) (Figure S5D).

Naïve mutants (n=8) and controls (n=9) in the acute phase were also subjected to a one-trial contextual active avoidance task as previously described (Cravens et al., 2006) with some modification. Briefly, the apparatus consisted of two compartments (light and dark) and further the dark compartment could be configured as one of two distinct contexts (Context X or Y) as shown in Figure S5E. On the training day, the time for the animals to cross from the right lit compartment to the dark Context X compartment was measured as the initial cross-latency. Once the animals were completely inside Context X, the door closed automatically and a single foot-shock (2 s, 0.12 mA) was administered as an unconditioned stimulus (US). Twenty four hours after training, the animals were placed into the dark compartment carrying Context Y (i.e., the unpaired context), and the door was automatically opened after 15 s to allow passage to the light compartment. The time for the animals to cross from the dark compartment to light after the door opened was measured as the reverse latency. One hour later, the same animals were placed into the dark compartment carrying US-paired Context X to again measure the reverse latency.

For cued fear conditioning, training consisted of a two-min acclimatization period to the context, followed by two pairings of a tone (8 kHz, 80 dB, 30 s) with a foot shock (0.85 mA, 2 s). Tone tests for cued fear memory were performed in a new context 24 hr after training. Pre-tone freezing was monitored 2.5 min prior to the presentation of the same tone for 30 s.

Open Field

Locomotor activity was recorded for 30 min using the automated Versamax Activity Monitoring System (AccuScan Institute, Columbus, OH) in a quiet and dimly illuminated room (50 lux in the center of open field). Total distance, vertical activity and time spent on central or peripheral areas in the chamber were automatically recorded for the analysis (Moy et al., 2007).

Elevated Plus Maze

The elevated plus-maze procedure was conducted as previously described (Belforte et al., 2010). Mutants (n=9, 17, and 12 for untreated, acute and chronic, respectively) and controls (n=10, 12, and 8 for untreated, acute and chronic, respectively) were individually placed on the center area, facing an open arm, and allowed to freely explore the apparatus for 5 min. Using the automated video tracking software ANY-maze (Stoelting, Wood Dale, IL), the number of entries into open or closed arms, and time spent in open or closed arms were evaluated.

Accelerating rotarod test

The accelerating rotarod test using an Accurotor rotarod (AccuScan Instruments) was conducted as previously described (Belforte et al., 2010).

Supplemental References

Buzsáki, G, Buhl, D.L., Harris, K.D., Csicsvari, J., Czéh, B., and Morozov, A. (2003). Hippocampal network patterns of activity in the mouse. Neuroscience *116*, 201-211.

Frotscher, M., Schlander, M., and Léránth, C. (1986). Cholinergic neurons in the hippocampus. A combined light- and electron-microscopic immunocytochemical study in the rat. Cell Tissue Res. *246*, 293-301.

Jiang, Z., Belforte, J.E., Lu, Y., Yabe, Y., Pickel, J., Smith, C.B., Je, H.S., Lu, B., and Nakazawa, K. (2010). eIF2α phosphorylation-dependent translation in CA1 pyramidal cells impairs hippocampal memory consolidation without affecting general translation. J. Neurosci. *30*, 2582-2594.

Lorente de No, R. (1934) Studies on the structure of the cerebral cortex. II. Continuation of the study of ammonic system. J. Psychol. Neurol. *46*, 113-177.

Moy, S.S., Nadler, J.J., Young, N.B., Perez, A., Holloway, L.P., Barbaro, R.P., Barbaro, J.R., Wilson, L.M., Threadgill, D.W., Lauder, J.M., Magnuson, T.R., and Crawley, J.N. (2007). Mouse behavioral tasks relevant to autism: phenotypes of 10 inbred strains. Behav. Brain Res. *176*, 4-20.

Penttonen, M., Kamondi, A., Sik, A., Acsády, L., and Buzsáki, G. (1997). Feed-forward and feed-back activation of the dentate gyrus in vivo during dentate spikes and sharp wave bursts. Hippocampus *7*, 437-450.

Sloviter, R.S. (1982). A simplified Timm stain procedure compatible with and routine of formaldehyde fixation paraffin embedding rat brain. Brain Res. Bull. *8*, 771-774.